Molecular Dynamics Study of Molten Lithium Iodide

S. Itoh*, M. Konagai, and K. Takahashi

Department of Electrical and Electronic Engineering, Tokyo Institute of Technology, O-okayama, Meguro-ku, Tokyo 152, Japan

Z. Naturforsch. **46a**, 155–159 (1991); received February 15, 1990

Dedicated to Dr. Karl Heinzinger on the occasion of his 60th birthday

The structural and dynamic properties of molten lithium iodide are investigated at two pressures (334 MPa at 784 K and 1054 MPa at 915 K), using molecular dynamics simulations with Born-Mayer-Huggins type pair potentials. On increasing the pressure, the local packing of the ions changes from tetrahedral to octahedral, the self-exchange velocity in the coordination shells decreases by a factor of 0.031, D_{Li} by a factor of 0.033 and D_I by a factor of 0.021.

Key words: Molecular dynamics, Liquid structure, LiI, Lithium iodide, Pressure.

1. Introduction

Data on the thermodynamic and transport properties of molten LiI are collected in Ref. [1]. Little is known, however, about the structure of this melt. There exists an X-ray diffraction study by Levy et al. [2] and some computational works, using the Born-Mayer-Huggins type potential [3], the Born type potential [4] and the exponential function divided by the fourth power of the distance for the repulsion [5].

In this work, Born-Mayer-Huggins pair potentials were used with a slight modification of the softness parameter, based on results obtained for the systems (Li–K)Cl and (Li–Na–K)Cl [6, 7]. The runs were performed for two molar volumes in order to investigate the effect of pressure.

2. Molecular Dynamics Simulation

216 Li and 216 I ions were placed in the periodic cube. The side length L was chosen to be either 2494.44 pm (low-density state) or 2331.18 pm (high-density state), corresponding to the molar volumes 43.27 and 35.32 cm^3/mol, respectively. The adopted pair potential consisted of the Coulombic term, the Born-type repulsive term and the two Huggins-Mayer type attractive terms, for which the Tosi and Fumi parameters [8] were used except for the softness parameter:

$$V_{ij}(r) = Z_i Z_j e^2/4\pi\varepsilon_0 r + (1 + Z_i/n_i + Z_j/n_j)\, b \cdot \exp[(\sigma_i + \sigma_j - r)/\varrho] - c_{ij}/r^6 - d_{ij}/r^8 .$$

Here, Z is the ionic charge number, e the elementary charge, ε_0 the permittivity of vacuum, n the number of electrons in the outer most shell, b a repulsion parameter, σ a value characteristic of the ion size and ϱ a softness parameter. ϱ was taken to be 0.92 times the value of Tosi-Fumi [8]. The values of the parameters are listed in Table 1. In the calculation of the Coulombic force, the Ewald method [9] was used with the cut-off distance in real space at $L/2$, the summation in reciprocal space for integers from 1 to 27, and the convergence parameter α equal to $5.6/L$. The time step was 4 fs. In the first MD simulation, the NTV ensemble at 760 K was used with a method slightly different [10] from that of Woodcock [11]. In the subsequent calcu-

Table 1. The parameters employed in the pair potentials.

	Li–Li	Li–I	I–I
$1 + Z_i/n_i + Z_j/n_j$	2.00	1.375	0.75
$c_{ij}/10^{-79}$ J m^6	0.073	3.30	378.0
$d_{ij}/10^{-99}$ J m^8	0.030	5.30	1060.0
$b = 0.338 \cdot 10^{-19}$ J, $\sigma_{Li} = 81.6$ pm		$\varrho = 0.92 \cdot 43.0 \cdot 10^{-8}$ m, $\sigma_I = 190.7$ pm	

* Present address: Department of Electronics and Information Science, The Nishi-Tokyo University, Yassawa, Uenohara-chou, Kitatsuru-gun, Yamanashi 409-01, Japan.

Reprint requests to Assoc. Prof. S. Itoh, Department of Electronics and Information Science, The Nishi-Tokyo University, Yassawa, Uenohara-chou, Kitaturu-gun, Yamanashi 409-01, Japan.

0932-0784 / 91 / 0100-0155 $ 01.30/0. – Please order a reprint rather than making your own copy.

Table 2. Conditions of the simulated LiI melts.

	Simulation (a)*	Simulation (b)**
$V/cm^3\,mol^{-1}$	43.27	35.32
P/MPa	334	1054
T/K	784	915
$E/kJ\,mol^{-1}$	−692	−700

* Side length of periodic cube containing 432 particles: 2494.44 pm.
** Side length of periodic cube containing 432 particles: 2331.18 pm.

Table 3. Characteristic values of the pair correlation functions $g(r)$ and coordination numbers $n_{ij}(r)$. R_i, r_{Mi}, and r_{mi} are the distances in pm where for the i-th time $g(r)$ crosses unity, has a maximum and a minimum, respectively.

	R_1	r_{M1}	$g(r_{M1})$	R_2	r_{m1}	$g(r_{m1})$	$n(R_2)$	$n(r_{m1})$
Simulation (a)								
Li–I	226	259	3.74	324	402	0.45	3.2	4.2
Li–Li	370	433	1.90	530	~611	0.67	9.3	12.7
I–I	380	429	2.41	522	~604	0.57	9.2	12.5
Simulation (b)								
Li–I	234	273	3.07	351	428	0.31	4.6	5.9
Li–Li	366	422	2.51	497	~597	0.61	10.2	14.2
I–I	375	421	3.15	490	~547	0.44	10.5	12.4

lations, the NEV ensemble was used, and after several thousand time steps for equilibration the data were collected. The total energies for the low- and high-density states are given in Table 2. The analyses were made with the last 12,000 steps (48 ps) and 10,500 steps (42 ps) for the low- and high-density states, respectively.

3. Results and Discussion

3.1. Static Properties

Figures 1 a and b represent the three partial pair distribution functions $g_{ij}(r)$ for molten LiI at the low and high density, respectively. Some characteristic values of the pair distribution functions are summarized in Table 3. At the high density, the first peaks of g_{++} and g_{--} are sharper and larger whereas that of g_{+-} is broader and smaller. Another remarkable feature of g_{+-} at the high density is the hump around 520 pm. We also observe that both g_{++} and g_{--} exhibit distorted oscillating profiles at the high density. The peaks of g_{--} are higher than those of g_{++} both at the low and high density states, and particularly the first peak height of g_{--} becomes comparable to that of g_{+-} at the high density. On increasing the density, the first peak of g_{+-} shifts to a longer distance and that of g_{++} and g_{--} shifts to a shorter distance. At the high density, the position of the second peaks of g_{--} and g_{++} is about $\sqrt{3}$-times that of the first peaks. The coordination numbers n_{++}, n_{+-}, and n_{--} increase with increasing density.

In Figs. 2, 3, and 4, the distributions of the partial coordination numbers of the cations and anions are illustrated. At the low density, the cation coordination distribution around the anion is similar to the anion coordination distribution around the cation (see Figure 2 a). At the high density, however, there is a significant difference between the coordination distributions of the anion and the cation. For the cation, the $n=5$ population is larger than the $n=4$ one, in contrast to the anion. The distribution for the high-density state clearly shifts to a higher value of n, compared with that for the low-density state, giving rise to a

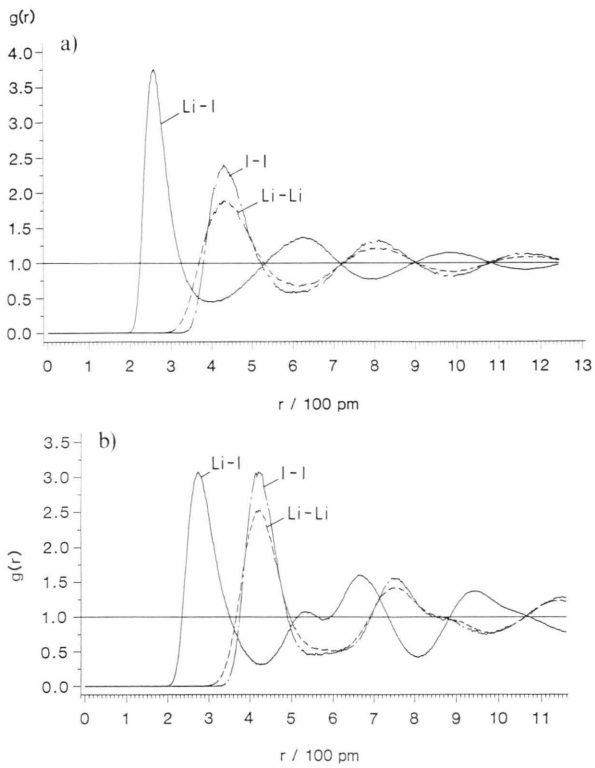

Fig. 1. The pair correlation functions g_{ij}, (a) at the low density, (b) at the high density.

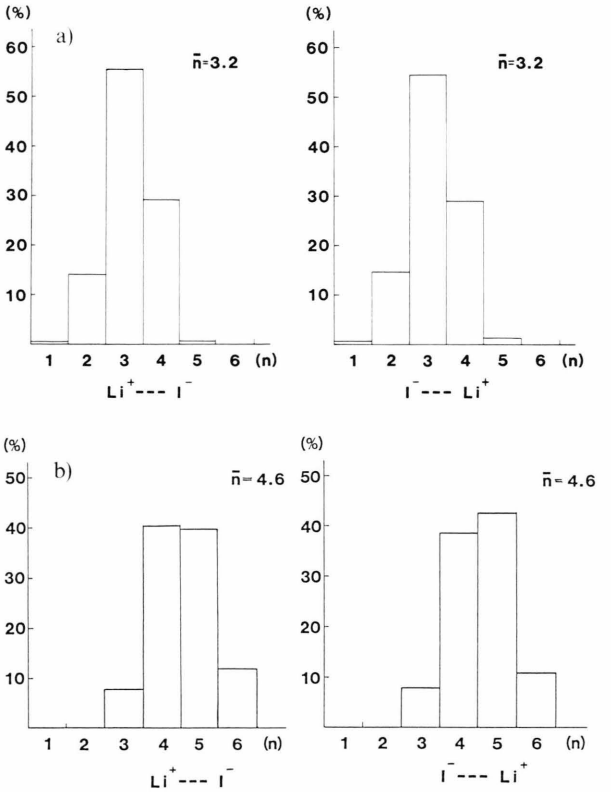

Fig. 2. The distribution of the coordination numbers of the oppositely charged ions within R_2, (a) at the low density, (b) at the high density.

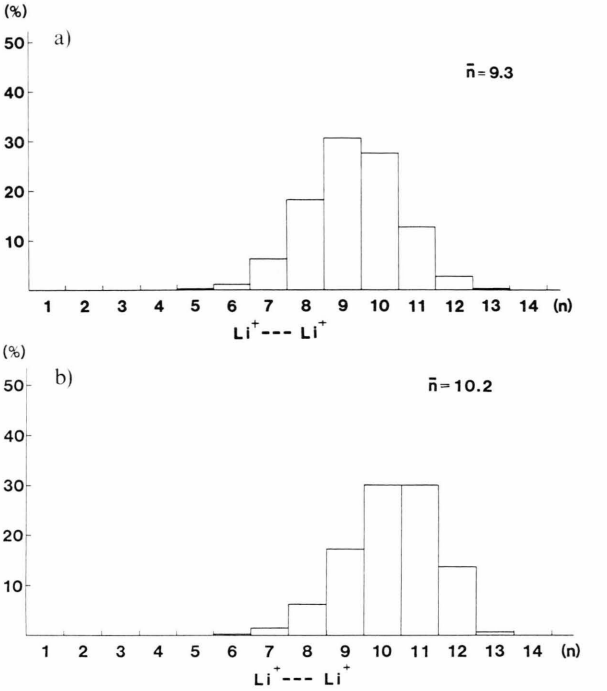

Fig. 3. The distribution of the coordination numbers of the lithium ion around the lithium ion within R_2, (a) at the low density, (b) at the high density.

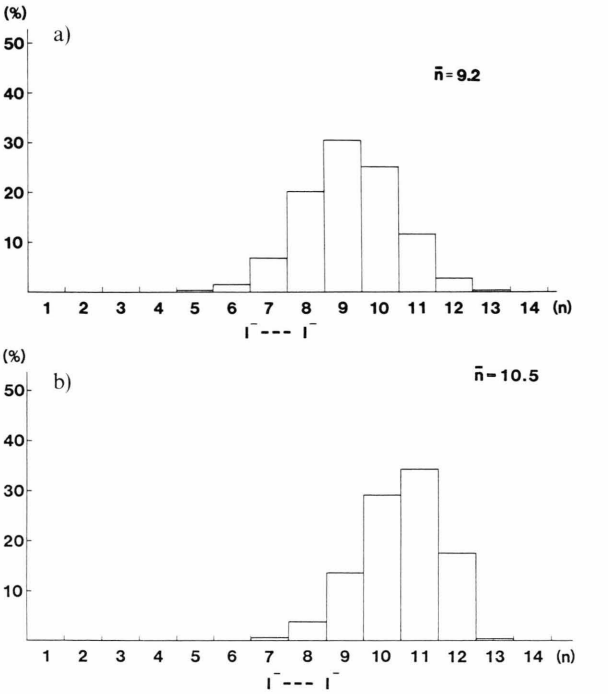

Fig. 4. The distribution of the coordination numbers of the iodide ion around the iodide ion within R_2, (a) at the low density, (b) at the high density.

higher average coordination number $\bar{n}$, as mentioned above (see Table 3). A similar tendency is found for the cation-cation (Fig. 3) and anion-anion (Fig. 4) coordination distributions.

Figures 5a and b represent for unlike ions the angular distribution functions defined as

$$P(\cos\theta) = -C\, dn(\cos\theta)/d\cos\theta,$$

where C is the normalization constant taken so that $\int_{-1}^{1} P(\cos\theta)\, d\cos\theta = 1$, and $dn(\cos\theta)$ is the number of ions around the cation or anion within the distance R_2 between $\theta - \delta\theta/2$ and $\theta + \delta\theta/2$ ($\delta\theta = 1°$). For the low-density state (Fig. 5a), a broad peak appears at 103° in both cases, suggesting a tetrahedral-like configuration of the opposite-ion packing around cations or anions. On the other hand, in the high-density state two distinct peaks appear at 90° and 180°. This reveals that local octahedral arrangements, similar to the NaCl-type crystal structure, are realized in the high-

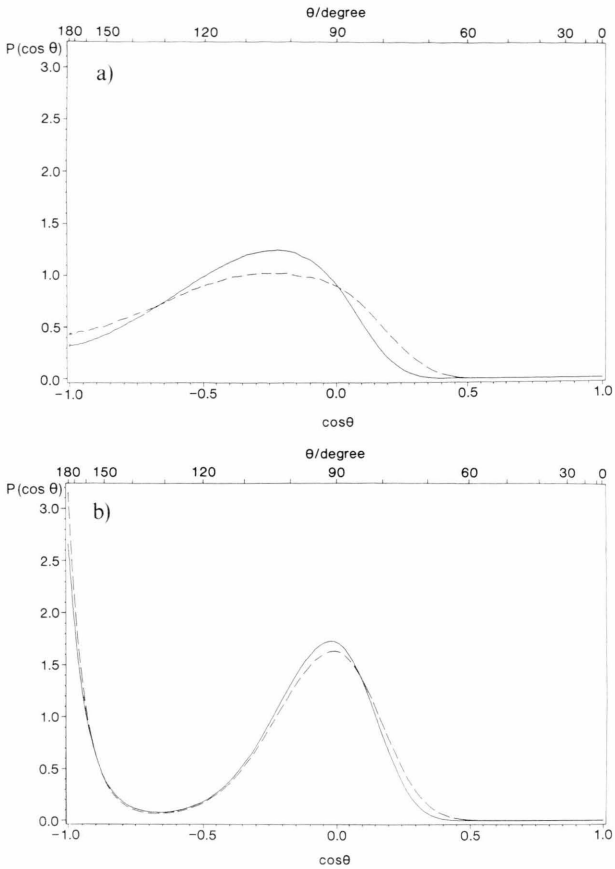

Fig. 5. The angular distribution function of I^- around Li^+ (solid line) and Li^+ around I^- (broken line), (a) at the low density, (b) at the high density.

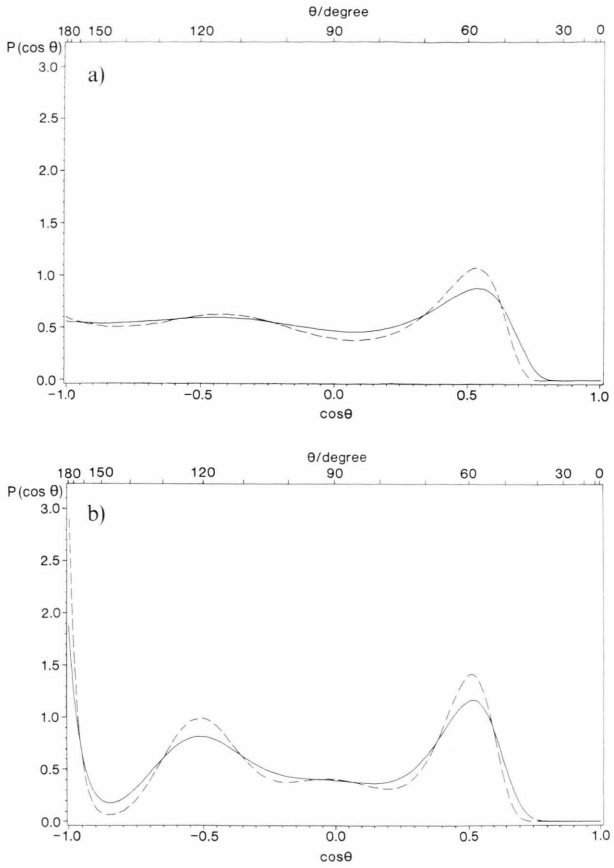

Fig. 6. The angular coefficient distribution function of Li^+ around Li^+ (solid line) and I^- around I^- (broken line), (a) at the low density, (b) at the high density.

density state, which is confirmed by the angular distribution functions of I^- around I^- and Li^+ around Li^+ shown in Figs. 6a and 6b. Distinct peaks appear at 60, 120, and 180° at the high density. The peak profile for iodide ions, which shows the expected peak at 90°, is clearer than that for lithium ions. Crystalline LiI has the NaCl-type structure. The first coordination number is 6 (octahedral configuration) at the distance of 300 pm at room temperature. The second coordination number is 12 at the distance $\sqrt{2} \times 300$ pm = 424 pm. The second nearest neighbor distance of the like ion pair is $\sqrt{3}$-times that of the first nearest neighbor distance. This striktly corresponds to the second peak position of the like ion pair appearing in Figure 1b. Thus, our result leads to the conclusion that at high density the local packing of the ions in molten LiI becomes similar to that in the crystal.

3.2. Dynamic Properties

The self-diffusion coefficients D in the LiI melt have been calculated from the mean square displacements according to the Einstein equation

$$D = (1/6\tau)\langle[r_i(t+\tau) - r_i(t)]^2\rangle,$$

where τ is a sufficiently long period for the mean square displacement to become a linear function of τ and the angle brackets represent the average over the ions (cations or anions) and 40 different time origins. For the low-density state, the self-diffusion coefficients of Li^+ and I^- were evaluated to be 5.78×10^{-5} and 2.25×10^{-5} cm^2 s^{-1}, respectively. The former value is consistent with the values 11.3×10^{-5} cm^2 s^{-1} derived from the conductivity and 3.11×10^{-5} cm^2 s^{-1} derived from NMR measurements, both at 742 K [12].

To our knowledge, experimental data on the self-diffusion coefficient of I^- in molten LiI do not exist. For the high-density state, the self-diffusion coefficients of Li^+ and I^- reduce to $0.192 \times 10^{-5}\,cm^2\,s^{-1}$ and $0.047 \times 10^{-5}\,cm^2\,s^{-1}$, respectively.

In order to examine another dynamic property of the LiI melt, we have computed the self-exchange velocity (SEV). The SEV measures an average velocity of the separating motion of pairs of ions with unlike signs and has been found to be well correlated with the internal mobility of molten alkali chlorides [13]. The SEV is defined as $(R_2 - \bar{r})/\tau$, where $\bar{r}$ is the average distance of the counterions within the distance R_2 from the ion, and τ is the time at which these counterions reach the average distance R_2 from the ion. The values of R_2 are listed in Table 3. The SEV was evaluated to be $77.3\,ms^{-1}$ for the low-density state and $2.38\,ms^{-1}$ for the high-density state. This suggests that the internal mobility is about 30 times smaller at the high density. In the calculation of the pressure effect on LiCl and LiBr [14] it has been found that the SEV decreases by a factor of 0.86 and 0.83, respectively, on increasing the pressurre by a factor of 10. In the present calculation, the increment of the pressure was only about 3-times, but the SEV decreased by a factor of 0.031.

The stronger tendency of molten LiI, compared to LiCl and LiBr, to become structured on increasing the pressure seems to be the reason for the spectacular decrease of the self-diffusion coefficients and the SEV, and thus the internal mobility of LiI on increasing the pressure. It would be interesting to check this prediction derived from computer simulations by measurements of the conductivity of molten LiI as a function of pressure.

Acknowledgements

One of the authors (S. I.) wishes to thank Professor I. Okada for his helpful discussions and Dr. A. Endoh for the computational assistance. She also wishes to express many thanks to Professor I. Ohmine for his encourageous advice.

Computer calculations have been carried out at the Institute for Molecular Science at Okazaki and at the Tokyo Institute of Technology. This work was supported by the joint program (1988–1989) of the Institute for Molecular Science.

[1] G. J. Janz, Molten Salts Handbook, Academic Press, New York 1967.
[2] H. A. Levy, P. A. Agron, M. A. Bredig, and M. D. Danford, Ann. New York Acad. Sci. **79,** 762 (1960).
[3] J. W. E. Lewis, K. Singer, and L. V. Woodcock, J. Chem. Soc. Faraday Trans. 2, **71,** 301 (1975).
[4] A. Baranyai, I. Ruff, and R. L. McGreevy, J. Phys. C: Solid State Phys. **19,** 453 (1986).
[5] J. Michielsen, P. Woerlee, F. V. D. Graaf, and J. A. A. Ketelaar, J. Chem. Soc. Faraday Trans. 2, **1975,** 1730.
[6] I. Okada, H. Okano, H. Ohtaki, and R. Takagi, Chem. Phys. Lett. **100,** 436 (1983).
[7] A. Endoh, T. Yamaguchi, I. Okada, and H. Ohtaki, Nippon Kagaku Kaishi **11,** 1492 (1986).
[8] F. G. Fumi and M. P. Tosi, J. Phys. Chem. Solids **25,** 31 (1964). – M. P. Tosi and F. G. Fumi, J. Phys. Chem. Solids **25,** 45 (1964).
[9] P. P. Ewald, Ann. Phys. **64,** 253 (1921).
[10] I. Okada, Y. Matsui, and Y. Kawamura, Nippon Kagaku Kaishi **1982,** 910.
[11] L. V. Woodcock, Chem. Phys. Lett. **10,** 257 (1971).
[12] F. van der Graaf, Ph.D. Thesis, Univ. Amsterdam (June 1981).
[13] S. Baluja, A. Endoh, and I. Okada, Z. Naturforsch. **43a,** 1065 (1988).
[14] I. Okada, A. Endoh, and S. Baluja, Z. Naturforsch. **46a,** 148 (1991).